Low Weber number jet collision regimes in microgravity

Francesc Suñol and Ricard González-Cinca
Department of Physics, Universitat Politècnica de Catalunya - BarcelonaTech, c/ E. Terradas 5, 08860 Castelldefels, Barcelona, Spain
(Dated: November 3, 2017)

The outcome of the collision between two liquid jets depends on the liquid properties, jet velocity and impact angle. So far studies on liquid jet impingement have been carried out in normal gravity conditions. In microgravity, jets are not accelerated and can show a different behavior than on ground. We perform an experimental analysis of the injection of liquid jets in microgravity, focusing in the jet impingement at different velocities and impact angles at low Weber number. Several regimes are obtained, some of which are not observable on ground. Other regimes take place at different parameters ranges than in normal gravity. A map of the observed regimes is proposed in terms of the Weber number and the impact angle.

PACS numbers: 47.55.df, 47.15.Uv, 47.55.N-

INTRODUCTION

The collision between two liquid jets can result in merging, bouncing, or dispersion in form of droplets [1–3]. The outcome of the collision can be controlled by changing two parameters, namely the flow rate and the impact angle of the colliding jets. Hence, the impinging jets configuration with changeable orientation becomes a simple and flexible method to enhance mixing. This configuration can be found in a variety of applications such as propellant injection in rocket engines, agrochemical coating, ink-jet printing, as well as in several pharmaceutical processes.

Most studies on liquid jets have focused on the description of the jet breakup mechanisms and the resulting droplet characteristics. The pioneering work of Lord Rayleigh on the linear stability analysis around the cylindrical base state was followed by numerous works considering non-linear effects that can become dominant in the breakup process. Very complete reviews of the underlying physics behind the jet breakup mechanisms can be found in Lin [4] and Eggers and Villermaux [5]. Three modes of liquid behaviour with their associated breakup mechanisms can take place in the laminar regime in normal gravity conditions: periodic dripping, chaotic dripping and jetting. Many attempts to model the breakup of liquid filaments or the transition between different regimes have been carried out [6–14]. Gravity force is neglected in most models, even though gravity can affect the jet breakup in cases like low surface tension fluids. Different modes of liquid jetting have been found in experiments in microgravity conditions [15, 16]. Umemura and Wakashima [17] and Tsukiji et al. [18] studied the atomization regimes of a liquid jet in weightlessness, as well as the effects of pressure and temperature. Suñol and González-Cinca [19, 20] reported a quantitative analysis of the breakup length, droplet size and jet structure in the breakup of a liquid jet in microgravity.

When two liquid jets collide, they can coalesce forming a new jet, a liquid chain or a sheet; bounce off each other; or disintegrate in the form of small droplets. The critical element determining merging versus bouncing is the dynamics of the air film that separates the colliding interfaces. Jets can attract and coalesce when the thickness of the film is reduced to the range of the intermolecular van der Waals forces (of the order of 100 nm). Li et al. [21] identified soft and hard merging mechanisms of colliding jets. In addition, they demonstrated that bouncing is confined to regimes of low Stokes number and high ratio between jet and capillary waves velocity. These regimes represent weak impact inertia and weak capillary effects, respectively. Given the dependence of these effects on liquid properties, bouncing in water was predicted to be non observable at atmospheric conditions. Wadha et al. [22] captured qualitatively the transition of colliding jets from bouncing to coalescence by means of a parameter determined by the Weber and Reynolds numbers as well as the angle of collision. All the studies carried out up until now belong to the inertia-dominated regime achieved under normal gravity conditions. The collision between liquid jets in microgravity conditions has not been addressed yet, even though the non-accelerated jets could give rise to new phenomenologies of potential interest for the design of space systems such as low-thrust satellite positioners and the operation of bipropellant rocket engines.

At high Weber number, the effects of gravity force on the collision between jets can be neglected since the acceleration generated to the jets is very low compared to the change in velocitiy caused by the collision. Thus, experiments in a microgravity environment are not expected to provide any new understanding on the characteristics of liquid jet collisions at high Weber number. However, at low Weber number, microgravity conditions are necessary to maintain the symmetry of the collision configuration.

In the present study, we analyze the injection of liquid jets in microgravity conditions, with a particular empha-

sis in the impingement of jets at different velocities and collision angles. Our aim is to determine the regimes that take place at low Weber number $\mathrm{We} = \rho d_n v^2/\sigma$, where ρ is the liquid density, d_n is the nozzle diameter, v is the velocity, and σ is the surface tension, and to compare them with results in normal gravity conditions.

EXPERIMENTAL SETUP

In order to carry out experiments in microgravity conditions, an experimental setup was designed to be used at the ZARM drop tower. In this platform, setups are placed inside an airtight capsule (1.5 m long and 80 cmwide) that is pulled up to a height of 120 meters at the top of the drop tube and released. After 4.74 s, the experiment lands in the deceleration unit filled with polystyrene pellets. During the free fall, the pressure inside the drop tube is 10^{-5} atm. The low air resistance allows the ZARM drop tower to provide a very good quality of microgravity of approximately $10^{-6} g_0$, where $g_0 = 9.81$ m/s^2 is the gravity acceleration at sea level.

Distilled water ($\rho = 998$ kg/m^3, $\sigma = 7.28 \cdot 10^{-2}$ N/m^2) was injected from two nozzles ($d_n = 1$ mm) at variable orientation and flow rate. The impact angle 2α of the jets was changed from 6° (quasi-parallel jets) to 180° (frontal collision). The flow rate at each nozzle Q varied from 5 to 100 ml/min, which corresponds to $0.5 \leq \mathrm{We} \leq 62$.

The flow rate was controlled and maintained by a high-accuracy liquid pump (Ismatec MCP-Z Standard), which assured a constant flow at each nozzle in microgravity conditions. A T-junction bifurcated the flow into two sub-lines, each of them connected to a manual valve that compensated any irregularities in the flow split at the T-junction. Images were recorded by means of a high-speed camera (Photron FastCam MC2) at 1000 fps with a resolution of 512x512 pixels each frame. Both the flow rate and the high-speed camera were controlled remotely using LabView software.

RESULTS AND DISCUSSION

The breakup length L_b of a single jet was obtained over $N = 500$ frames for every Q, and the average value $\langle L_b \rangle = \frac{1}{N} \sum_{i=1}^{N} L_{bi}$ was calculated. The breakup length shows a linear behaviour with the jet velocity (hence with $\sqrt{\mathrm{We}}$) at a wide range of flow rates [4].

Figure 1 shows the normalized average breakup length as a function of $\sqrt{\mathrm{We}}$. Labels "a" and "b" correspond to the dripping regime, in which the injected droplet remains attached to the nozzle. In "a", inertia is negligible and the droplet shape remains approximately spherical. As the flow rate increases, inertia forces slightly prevail over surface tension, which makes the droplet to adopt

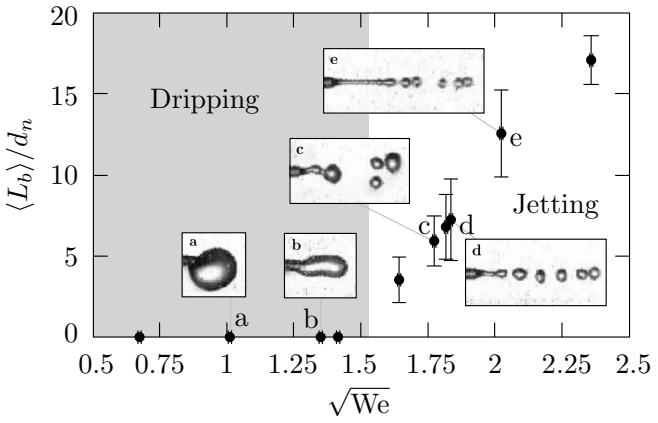

FIG. 1. Normalized average breakup length as a function of $\sqrt{\mathrm{We}}$. "a" and "b" correspond to the dripping regime (liquid mass attached to the nozzle), while "c", "d" and "e" correspond to the jetting regime.

an irregular elongated shape ("b"). When inertia overcomes surface tension, a liquid jet is formed ("c", "d" and "e" in Fig. 1). The transition from dripping to jetting occurs at a critical Weber ($\mathrm{We}_{cr} \approx 2.3$). At low flow rates in the jetting regime ($\mathrm{We} \gtrsim \mathrm{We}_{cr}$), the droplet size and generation frequency are highly unpredictable ("c"). As the flow rate increases, the droplets generated from the jet breakup become smaller and with a lower size dispersion ("d" and "e"). In this case, the average jet breakup length increases linearly with the square root of the Weber number [20].

A wide range of regimes emerge as a result of the oblique and frontal jet interactions (see in Table I all the cases studied, where v is the liquid injection velocity). Figure 2 shows the regimes obtained in the oblique jet interaction. In Figs. 2a and 2d, a nonuniform spatial distribution of noncoalescing droplets is generated. Figs. 2b and 2e show droplets from different jets coalescing with each other. Soft merging between low velocity jets with a sudden bend of the jets very close to the merging point can be observed in Figs. 2c and 2f. Hard merging takes place at high impact inertia, giving rise to a liquid chain (Fig. 2g) or a sheet (Fig. 2h and 2i). At low values of 2α used ($6° \leq 2\alpha \leq 22°$), jets bounced off each other with an outgoing angle 2ϕ smaller than the impact angle (Figure 2j). The non coalescence between jets can be related to the behaviour of the film of air separating both interfaces as they come close to each other, as found in [22]. Jets drag along air into the collision region, where it is squeezed in a thin film. Since the thickness of the air film is much smaller than the other dimensions, lubrication approximation is applicable, which results in high magnitude forces keeping the jets apart. As soon as the air between jets is drained out, coalescence could take place.

The transition from jet bouncing to coalescence is il-

Fig#	2α (degrees)	v (m/s)	Regime
2a	82	0.49	Droplet bouncing
2b	82	0.55	Droplet coalescence
2c	82	0.74	Jet coalescence
2d	14	0.49	Droplet bouncing
2e	14	0.53	Droplet coalescence
2f	14	0.59	Jet coalescence
2g	30	2.12	Liquid chain
2h	90	1.34	Liquid chain/sheet
2i	90	2.12	Liquid sheet
2j	10	0.68	Jet bouncing
3	22	0.68	Jet coalescence/bouncing
6a	180	0.38	Dripping
6b	180	0.45	Droplet bouncing
6c	180	0.47	Droplet bouncing
6d	180	0.64	Jet coalescence
	6	0.62	Jet coalescence
	6	0.85	Jet coalescence/bouncing
	53	0.70	Jet coalescence
	180	0.49	Droplet coalescence
	180	0.53	Droplet coalescence
	180	0.91	Jet coalescence
	180	2.12	Liquid sheet

TABLE I. List of analyzed cases.

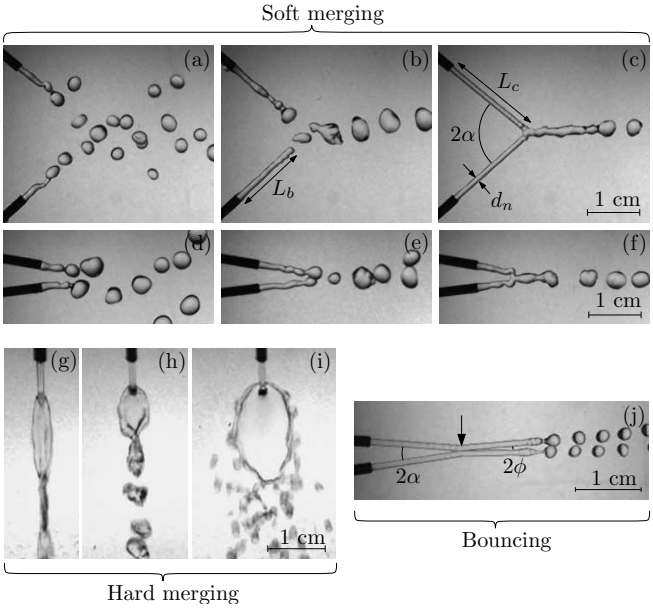

FIG. 2. Snapshots of different regimes when oblique jets are injected. (a) and (d) droplet bouncing; (b) and (e) droplet coalescence; (c) and (f) jet coalescence; (g) liquid chain; (h) and (i) liquid sheet; (j) jet bouncing. (a)-(f) soft merging; (g)-(i) hard merging.

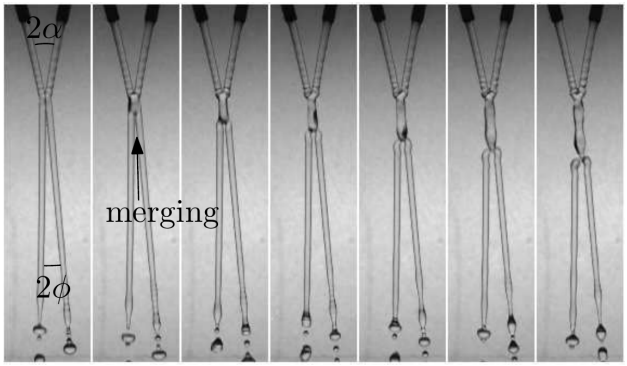

FIG. 3. Series of snapshots showing the transition from bouncing to coalescing jets. Time interval between consecutive frames is 1 ms.

lustrated in Fig. 3. The bouncing regime corresponds to a metastable state, and coalescence is triggered by an instability in the interface of the colliding jets. A film of air is entrained by the liquid flow and is continuously replenished, resulting in a self-sustained noncoalescence. However, a sufficiently large perturbation in the jet flow (which can be due to nozzle vibrations, pump anomalous operation, or the presence of a colloid in the liquid) can force the air to quickly drain out giving rise to coalescence.

Due to the symmetry of the problem, the dynamics of the air layer between colliding jets is analogous to that of the droplet impact on solid surfaces [21]. The width of the air layer H_d scales with the dimensionless impact velocity as $H_d/R = A_I \mathrm{St}^{-2/3}$, where $R = d_n/2$, A_I is a prefactor, and St is the Stokes number, defined as $\mathrm{St} = \rho R v/\eta_g$, where $\eta_g = 1.983 \cdot 10^{-5}$ Pa s is the air viscosity. When oblique collisions are considered, the impact velocity is modified by a $\sin\alpha$ factor. Thus, the Stokes number becomes $\mathrm{St} = \rho d_n v \sin\alpha/(2\eta_g)$. According to Li *et al.* [21], there is a critical value of the Stokes number that determines the transition from bouncing to merging. At low jet velocities, the shape of the jet is not cylindrical due to the reflected waves to the nozzle. The velocity of the capillary waves is estimated as $v_c \approx (\sigma k/\rho)^{1/2}$, where k is the wavenumber and is of the order of $1/R$. The ratio between the jet velocity and the capillary waves velocity leads to a second dimensionless number Γ, defined as $\Gamma = v/v_c = v(\rho R/\sigma)^{1/2}$, which controls the bouncing/merging transition at low jet velocities [21]. Therefore, the jet bouncing and coalescence regimes can be analyzed by means of the Stokes number St and the ratio between jet and capillary waves velocity Γ. Fig. 4 shows St as a function of Γ. Crosses correspond to coalescence, circles to bouncing, and crosses inside circles to a metastable bouncing state like the one shown in Fig. 3. Jet bouncing was found only at $\Gamma > 0.2$ in [21]. However, two of the observed bouncing regimes in our experiments took place at $\Gamma < 0.2$. Therefore, microgravity conditions seem to favour bouncing against coalescence. Bouncing is enhanced in microgravity since jets are not accelerated and hence the removal of air between them becomes more difficult.

The transition from bouncing to coalescence can be analyzed in terms of the parameter K, defined as

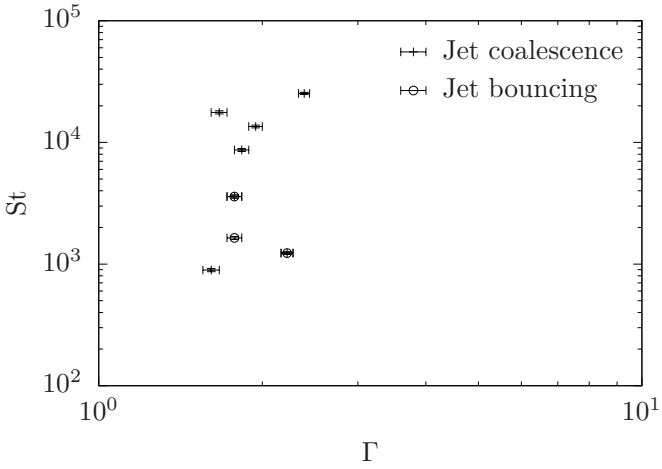

FIG. 4. Stokes number as a function of the ratio between jet and capillary waves velocity.

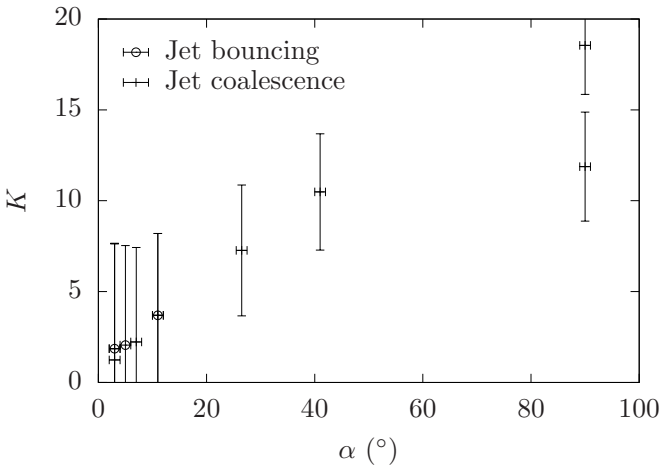

FIG. 5. $K = (\mathrm{We}_\alpha \sqrt{\mathrm{Re}_\alpha}/\sin\alpha)^{1/2}$ as a function of the impact angle.

$K = (\mathrm{We}_\alpha \sqrt{\mathrm{Re}_\alpha}/\sin\alpha)^{1/2}$, where $\mathrm{We}_\alpha = \mathrm{We}\sin^2\alpha$ and $\mathrm{Re}_\alpha = v d_n \sin\alpha/\nu$, ν being the kinematic viscosity. The introduction of the dimensionless numbers We_α and Re_α comes when considering oblique collisions, since the impact velocity becomes $v\sin\alpha$. Wadhwa et al. observed coalescence at $K > K_{cr}$ and bouncing at $K < K_{cr}$, with $K_{cr} = 6.1$ [22]. Fig. 5 shows the behaviour of K as a function of α for the cases of jet bouncing and coalescence observed here, where a cross inside a circle corresponds to a metastable bouncing state. Our results show several cases of jet coalescence at $K < 6.1$ at $\alpha < 10^o$, which is a region not explored in [22]. In this region jets are quasi-parallel and small interfacial instabilities can generate coalescence more easily than at large values of α. In fact, one would expect that in normal gravity conditions this effect is enhanced and that K_{cr} substantially decreases as $\alpha = 0^o$ is approached.

The frontal collision between two jets provides particular features since the system is axisymmetric and the outcome of the collision is located in the injection axis. As a consequence, the resulting fluid body interacts with the incoming liquid streams, as opposed to the oblique jets case, in which the result of the collision moves away from the collision point. Fig. 6 shows the regimes observed in the opposed-jets configuration, with a separation between nozzle tips of 6 cm. Fig. 6a shows the dripping regime that takes place at low We, in which surface tension dominates over fluid inertia and droplets grow remaining attached to the nozzles. In Figs. 6b to 6d, $\mathrm{We} > \mathrm{We}_{cr}$ and the jetting mode is attained. Fig. 6b shows the dispersion of droplets generated from jet atomization occurring close to the nozzle. Droplets approach each other at a relative velocity around 10 cm/s and bounce off since the time scale of draining the air film between the two interfaces is higher than the contact time between droplets. At higher jet velocities, the inertia of the colliding droplets generates strong perturbations of the air gap between liquid interfaces, forcing them to coalesce. In this case, a central droplet is formed and grows from coalescence with incoming droplets (Fig. 6c). The jet breakup length increases with increasing flow rate. When L_b is larger than the distance from the nozzle tip to the colision point, jets coalesce before atomization can take place, and a liquid bridge is formed (Fig. 6d). The interaction between jets creates a central liquid body that connects the two nozzles permanently. The shape of the liquid bridge highly depends on the flow rate. At low flow rates, the bridge shape oscillates between oblate and prolate spheroids. At large flow rates, the central body becomes a steady liquid sheet.

To characterize the conditions under which the observed regimes take place, a map in terms of the Weber number and the impact angle is proposed (Fig. 7). The regimes represented, ordered by increasing flow rate, are: dripping, droplet bouncing, droplet coalescence, jet coalescence, jet bouncing, liquid chain, and liquid sheet. Some of the regimes, such as jet bouncing or liquid chains, occur only in configurations with $2\alpha \neq 0, \pi$ rad. Jet coalescence is observed at $\alpha = 0$ rad as a result of the soft merging mechanism.

CONCLUSIONS

In conclusion, our results significantly extend the understanding of the behavior of liquid jets at low Weber numbers. We have analyzed the impingement of jets in microgravity conditions in a large range of impact angle including frontal collision, and observed several regimes. Some of the regimes take place at different parameters ranges that in normal gravity conditions, while others occur only in microgravity. A map of the identified regimes have been proposed in terms of the Weber number and the impact angle.

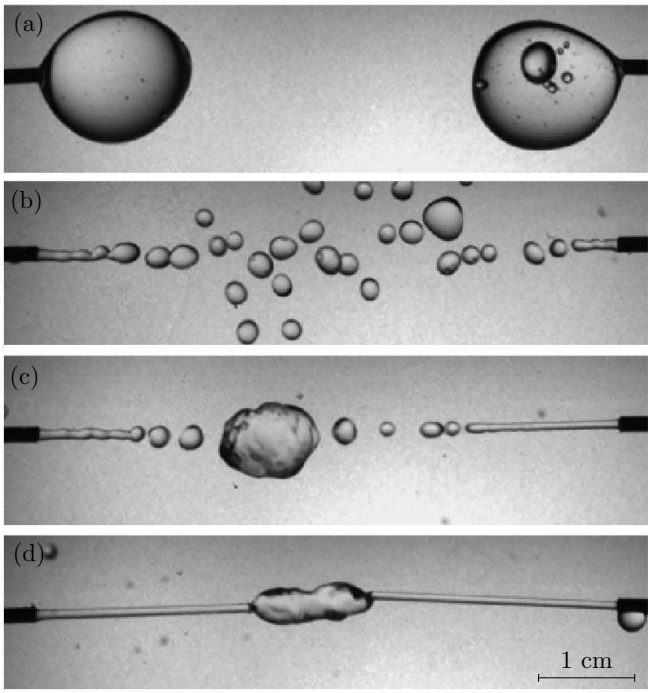

FIG. 6. Regimes observed in the opposed-jets configuration: (a) dripping; (b) droplet bouncing; (c) droplet coalescence; (d) jet coalescence.

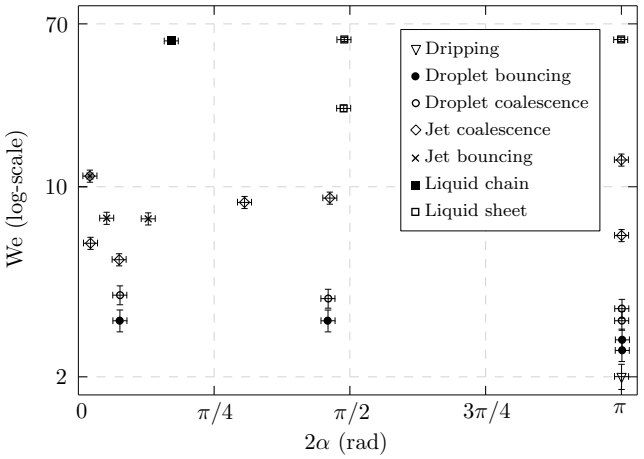

FIG. 7. Jet collision regimes in terms of We and the impact angle.

ACKNOWLEDGEMENTS

This research was supported by the Spanish *Ministerio de Economía y Competitividad, Secretaría de Estado de Investigación, Desarrollo e Innovación* (project number AYA2012-34131), and by the *Agencia Estatal de Investigación* and EU FEDER (project number ESP2016-79196-P). We acknowledge ESA for providing access to the ZARM drop tower, and ZARM engineers for their technical assistance.

[1] Y.J. Choo and B.S. Kang, "A study on the velocity characteristics of the liquid elements produced by two impinging jets," Experiments in Fluids **34**, 655–661 (2003).
[2] Sungjune Jung, Stephen D. Hoath, Graham D. Martin, and Ian M. Hutchings, "Atomization patterns produced by the oblique collision of two newtonian liquid jets," Physics of Fluids **22**, 042101 (2010).
[3] Navish Wadhwa and Sunghwan Jung, "Non-coalescence of jets," Physics of Fluids **23**, 091105 (2011).
[4] S. P. Lin, *Breakup of liquid sheets and jets* (Cambridge University Press, 2003).
[5] Jens Eggers and Emmanuel Villermaux, "Physics of liquid jets," Reports on Progress in Physics **71**, 036601 (2008).
[6] R. D. Reitz and F. V. Bracco, "Mechanism of atomization of a liquid jet," Physics of Fluids **25**, 1730–1742 (1982).
[7] S. J. Leib and M. E. Goldstein, "Convective and absolute instability of a viscous liquid jet," Physics of Fluids **29**, 952–954 (1986).
[8] S. P. Lin and Z. W. Lian, "Absolute instability of a liquid jet in a gas," Physics of Fluids **1**, 490–493 (1989).
[9] S. P. Lin and R. D. Reitz, "Drop and spray formation from a liquid jet," Annual Review of Fluid Mechanics **30**, 85–105 (1989).
[10] Bala Ambravaneswaran, Hariprasad J. Subramani, Scott D. Phillips, and Osman A. Basaran, "Dripping-jetting transitions in a dripping faucet," Phys. Rev. Lett. **93**, 034501 (2004).
[11] Wim van Hoeve, Stephan Gekle, Jacco H. Snoeijer, Michel Versluis, Michael P. Brenner, and Detlef Lohse, "Breakup of diminutive rayleigh jets," Physics of Fluids **22**, 122003 (2010).
[12] J. M. Montanero, M. A. Herrada, C. Ferrera, E. J. Vega, and A. M. Gañán Calvo, "On the validity of a universal solution for viscous capillary jets," Physics of Fluids **23**, 122103 (2011), http://dx.doi.org/10.1063/1.3670007.
[13] A. M. Gañán Calvo, C. Ferrera, and J. M. Montanero, "Universal size and shape of viscous capillary jets: application to gas-focused microjets," Journal of Fluid Mechanics **670**, 427–438 (2011).
[14] Alfonso A. Castrejón-Pita, J. R. Castrejón-Pita, and I. M. Hutchings, "Breakup of liquid filaments," Phys. Rev. Lett. **108**, 074506 (2012).
[15] A. P. R. Edwards, B. P. Osborne, J. M. Stoltzfus, T. Howes, and T. A. Steinberg, "Instabilities and drop formation in cylindrical liquid jets in reduced gravity," Physics of Fluids **14**, 3432–3438 (2002).
[16] Barnaby Osborne and Theodore Steinberg, "An experimental investigation into liquid jetting modes and breakup mechanisms conducted in a new reduced gravity facility," Microgravity Science and Technology **18**, 57–61 (2006).
[17] Akira Umemura and Yuichiro Wakashima, "Atomization regimes of a round liquid jet with near-critical mixing surface at high pressure," Proceedings of the Combustion Institute **29**, 633 – 640 (2002).
[18] H. Tsukiji, A. Umemura, and M. Hisida, "Micro-gravity research on the atomization mechanism of near-critical mixing surface jet," Proceedings of the Conference on Aerospace Propulsion **44**, 97–101 (2004).

[19] Francesc Suñol and Ricard González-Cinca, "Droplet collisions after liquid jet breakup in microgravity conditions," Journal of Physics: Conference Series **327**, 012026 (2011).

[20] Francesc Suñol and Ricard González-Cinca, "Liquid jet breakup and subsequent droplet dynamics under normal gravity and in microgravity conditions," Physics of Fluids **27**, 077102 (2015).

[21] Minglei Li, Abhishek Saha, D. L. Zhu, Chao Sun, and Chung K. Law, "Dynamics of bouncing-versus-merging response in jet collision," Phys. Rev. E **92**, 023024 (2015).

[22] Navish Wadhwa, Pavlos Vlachos, and Sunghwan Jung, "Noncoalescence in the oblique collision of fluid jets," Phys. Rev. Lett. **110**, 124502 (2013).